Transp Porous Med (2010) 85:723–741
DOI 10.1007/s11242-010-9588-6

Stability of Flow with Viscous Dissipation in a Horizontal Porous Layer with an Open Boundary Having a Prescribed Temperature Gradient

A. Barletta · L. Storesletten

Received: 25 March 2010 / Accepted: 26 April 2010 / Published online: 20 May 2010

Abstract A buoyancy-induced stationary flow with viscous dissipation in a horizontal porous layer is investigated. The lower boundary surface is impermeable and subject to a uniform heat flux. The upper open boundary has a prescribed, linearly varying, temperature distribution. The buoyancy-induced basic velocity profile is parallel and non-uniform. The linear stability of this basic solution is analysed numerically by solving the disturbance equations for oblique rolls arbitrarily oriented with respect to the basic velocity field. The onset conditions of thermal instability are governed by the Rayleigh number associated with the prescribed wall heat flux at the lower boundary, by the horizontal Rayleigh number associated with the imposed temperature gradient on the upper open boundary, and by the Gebhart number associated with the effect of viscous dissipation. The critical value of the Rayleigh number for the onset of the thermal instability is evaluated as a function of the horizontal Rayleigh number and of the Gebhart number. It is shown that the longitudinal rolls, having axis parallel to the basic velocity, are the most unstable in all the cases examined. Moreover, the imposed horizontal temperature gradient tends to stabilise the basic flow, while the viscous dissipation turns out to have a destabilising effect.

Keywords Porous layer · Open boundary · Prescribed temperature gradient · Viscous dissipation · Buoyant flow · Thermal instability

1 Introduction

A fluid saturated porous medium may become thermally unstable when its lower boundary is either heated with a prescribed heat flux or kept at a temperature higher than the

A. Barletta (✉)
DIENCA, Alma Mater Studiorum—Università di Bologna, Via dei Colli 16, 40136 Bologna, Italy
e-mail: antonio.barletta@unibo.it

L. Storesletten
Department of Mathematics, University of Agder, Postboks 422, 4604 Kristiansand, Norway
e-mail: leiv.storesletten@uia.no

upper boundary. The onset conditions for the instability, developed with a strong analogy to the well-known Rayleigh–Bénard problem, have been extensively studied over the past few decades starting from the pioneering studies by Horton and Rogers (1945) and by Lapwood (1948). Exhaustive reviews of this subject and of its manifold generalisations can be found in Nield and Bejan (2006), Rees (2000) and Tyvand (2002). The studies of Horton and Rogers (1945) and Lapwood (1948) were devoted to the stability analysis of a basic state of vanishing velocity. These investigations were extended by Prats (1996) by considering a basic parallel and uniform velocity profile. Further developments were carried out by extending the analysis beyond the domain of validity of Darcy's law, for instance, including the effects of the fluid inertia (Rees 1997) or applying the Brinkman model (Rees 2002).

An important feature of the Prats problem (Prats 1996) is that the uniform basic velocity profile is caused by an externally imposed horizontal pressure gradient. On the other hand, the basic flow may be utterly caused by the buoyancy effect and, in this case, it is non-uniform (Barletta et al. 2010). This recent article (Barletta et al. 2010) shows that the basic non-uniform flow in the porous medium may become unstable when the horizontal Rayleigh number, i.e. the Rayleigh number associated with the imposed horizontal temperature gradient on the upper boundary, exceeds a critical value. The analysis carried out by Barletta et al. (2010) refers to a porous layer with an impermeable adiabatic lower boundary, and an impermeable upper boundary where a linearly changing temperature is prescribed.

The interest in the analysis of buoyant flows associated with a horizontal or inclined temperature gradient originates from the models for the distribution of winds in the atmosphere, generally known as Hadley circulation. These buoyant flows are of interest also for understanding the hydrodynamical aspects of crystal growth in the core of a large cavity in horizontal Bridgman configurations (Laure and Roux 1989). Stability studies of the Hadley flow in a horizontal porous layer induced by a linearly varying boundary temperature were first carried out by Weber (1974). A comprehensive review on this subject may be found in Nield and Bejan (2006).

The aim of the present article is to develop the analysis of the possible instability of a buoyancy-induced basic flow in a porous layer with an open boundary at constant pressure. In analogy with Barletta et al. (2010), the effect of viscous dissipation is taken into account. On the other hand, unlike in Barletta et al. (2010), the lower impermeable surface is considered as subject to a uniform wall heat flux. The instability of porous layers with an open boundary has been the subject of several investigations in the past decades. Nield (1968) proved that the critical Rayleigh number for the onset of convective instability in a porous layer with a lower impermeable boundary at a uniform temperature and an upper open boundary at a uniform heat flux is π^2, and not $4\,\pi^2$ as for the classical Horton, Rogers and Lapwood problem (Horton and Rogers 1945; Lapwood 1948), where the upper boundary is assumed impermeable and isothermal. Nield's critical condition was in fact previously reported by Elder (1967), but this author omitted to mention that the critical value π^2 holds only if the impermeable boundary is at a uniform temperature, while the open boundary is at a uniform heat flux. More recently, Lu et al. (1999) pointed out that the critical value of the Rayleigh number can be significantly smaller than π^2 if one refers to a moist gas saturated porous medium and if the usual Oberbeck–Boussinesq approximation is relaxed. McKibbin (1986) investigated the onset conditions of convective rolls in a porous layer bounded by isothermal surfaces. In the present article, the upper open boundary is assumed to be subject to a general hydrodynamic condition that includes the usual constant pressure condition as a special limiting case. Tyvand (2002) clarified that the condition of an open boundary describes an interface between a fluid-saturated porous medium and its saturating fluid in a condition of hydrostatic pressure distribution. This author claims that this model of the open

boundary is more realistic than the usual constant pressure condition. In the present article this distinction has no effects. In fact, we assume a constant pressure condition at the upper boundary. Nevertheless, we find that the tangential components of the seepage velocity vector vanish at the upper boundary, in perfect agreement with Tyvand's model (Tyvand 2002).

2 Mathematical Model

We study a fluid saturated porous layer with an upper open boundary $\overline{y} = \ell$ and a lower impermeable boundary $\overline{y} = 0$. The $\overline{y}$-axis is oriented vertically such that $\mathbf{g} = -g\,\mathbf{e}_y$, where g is the modulus of the gravitational acceleration, $\mathbf{g}$, and $\mathbf{e}_y$ is the unit vector in the $\overline{y}$-direction. Here, the overline is used to denote the dimensional coordinates, $(\overline{x}, \overline{y}, \overline{z})$, the dimensional seepage velocity field, $\overline{\mathbf{u}} = (\overline{u}, \overline{v}, \overline{w})$, the dimensional temperature field, $\overline{T}$, and the dimensional pressure field, $\overline{p}$, as well as the dimensional gradient operator, $\overline{\nabla}$, and the dimensional Laplacian operator, $\overline{\nabla}^2$. We assume that the lower boundary is heated with a uniform heat flux q_0, while the upper open boundary $\overline{y} = \ell$ is subject to a linearly varying temperature in an arbitrary horizontal direction. A sketch of the porous layer and of the coordinate frame is given in Fig. 1. The mathematical model adopted is based on Darcy's law and on the Oberbeck–Boussinesq approximation. The viscous dissipation contribution is included in the local energy balance. Thus, the governing equations can be written as

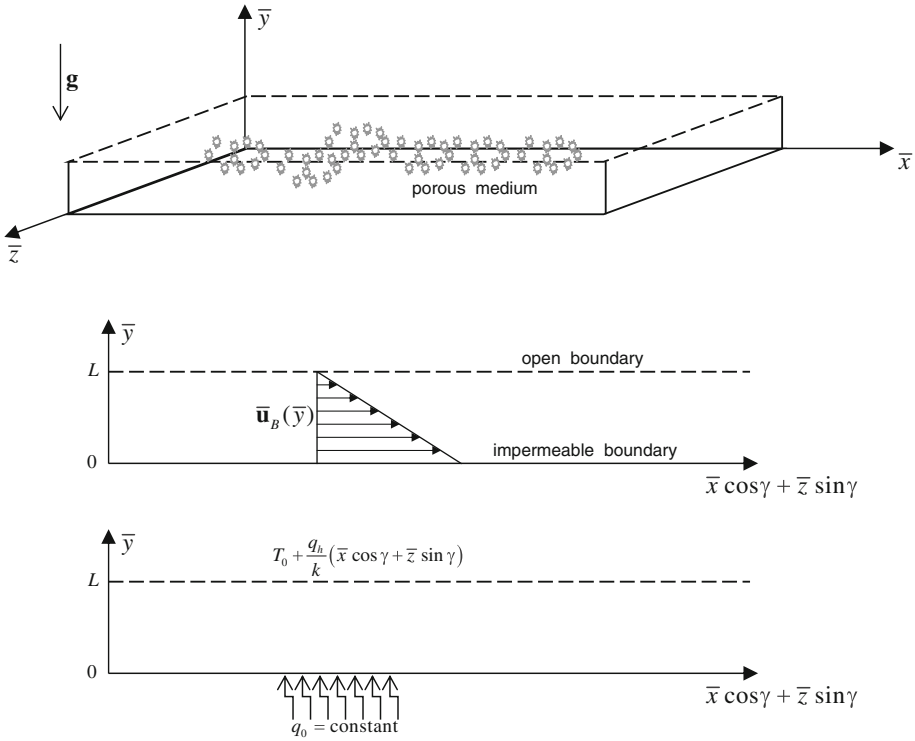

Fig. 1 A sketch of the porous layer, of the basic flow and of the boundary conditions

$$\overline{\nabla} \cdot \overline{\mathbf{u}} = 0, \tag{1}$$

$$\frac{\mu}{K}\,\overline{\mathbf{u}} = -\overline{\nabla}\overline{p} + \rho\, g\, \beta\, \left(\overline{T} - T_0\right) \mathbf{e}_y, \tag{2}$$

$$\sigma\, \frac{\partial \overline{T}}{\partial \overline{t}} + \overline{\mathbf{u}} \cdot \overline{\nabla}\, \overline{T} = \alpha\, \overline{\nabla}^2 \overline{T} + \frac{\nu}{K\, c}\, \overline{\mathbf{u}} \cdot \overline{\mathbf{u}}, \tag{3}$$

where μ is the dynamic viscosity, K is the permeability, ρ is the fluid density at the reference temperature T_0, β is the coefficient of thermal expansion, σ is the ratio between the average volumetric heat capacity of the fluid saturated porous medium and the volumetric heat capacity of the fluid, α is the effective thermal diffusivity, ν is the kinematic viscosity and c is the heat capacity per unit mass of the fluid. A study on the appropriate definition of c in the framework of the Oberbeck–Boussinesq approximation has been recently carried out by Barletta (2009).

The boundary conditions are

$$\overline{y} = 0: \quad \overline{v} = 0, \quad \frac{\partial \overline{T}}{\partial \overline{y}} = -\frac{q_0}{k}, \tag{4}$$

$$\overline{y} = \ell: \quad \overline{p} = p_0, \quad \overline{T} = T_0 + \frac{q_\mathrm{h}}{k}\, (\overline{x}\, \cos\gamma + \overline{z}\, \sin\gamma)\,. \tag{5}$$

In Eq. 5, k is the effective thermal conductivity, q_h is the imposed horizontal heat flux and γ is the inclination angle of the horizontal temperature gradient with respect to the $\overline{x}$-axis.

2.1 Nondimensional Formulation

The governing Eqs. 1–5 can be rewritten in a nondimensional form as

$$\nabla \cdot \mathbf{u} = 0, \tag{6}$$

$$\mathbf{u} = -\nabla p + T\, \mathbf{e}_y, \tag{7}$$

$$\frac{\partial T}{\partial t} + \mathbf{u} \cdot \nabla T = \nabla^2 T + Ge\, \mathbf{u} \cdot \mathbf{u}, \tag{8}$$

$$y = 0: \quad v = 0, \quad \frac{\partial T}{\partial y} = -\,Ra, \tag{9}$$

$$y = 1: \quad p = 0, \quad T = Ra_\mathrm{h}\, (x \cos\gamma + z \sin\gamma)\,. \tag{10}$$

Here, we notice that the boundary condition $p = 0$ at $y = 1$ can be equivalently replaced by

$$y = 1: \quad u = 0 = w, \tag{11}$$

as it can be easily inferred from the local momentum balance Eq. 7.
The nondimensional variables are defined such that

$$(\overline{x}, \overline{y}, \overline{z}) = (x, y, z)\, \ell, \quad \overline{t} = t\, \frac{\sigma\, \ell^2}{\alpha}, \quad (\overline{u}, \overline{v}, \overline{w}) = (u, v, w)\, \frac{\alpha}{\ell},$$
$$\overline{T} = T_0 + T\, \frac{\nu\, \alpha}{K\, \beta\, g\, \ell}, \quad \overline{p} = p_0 + p\, \frac{\mu\, \alpha}{K}, \tag{12}$$

while the nondimensional parameters are given by

$$Ge = \frac{\beta\, g\, \ell}{c}, \qquad Ra = \frac{g\, \beta\, q_0\, K\, \ell^2}{\nu\, \alpha\, k}, \qquad Ra_{\mathrm{h}} = \frac{g\, \beta\, q_{\mathrm{h}}\, K\, \ell^2}{\nu\, \alpha\, k}. \tag{13}$$

Here, Ge is the Gebhart number, Ra is the Rayleigh number, and Ra_{h} is the horizontal Rayleigh number associated with the horizontal temperature gradient.

3 Basic Solution

There exists a steady basic solution of Eqs. 6–10, given by

$$u_{\mathrm{B}}(y) = Ra_{\mathrm{h}}\,(1-y)\cos\gamma, \qquad v_{\mathrm{B}} = 0, \qquad w_{\mathrm{B}}(y) = Ra_{\mathrm{h}}\,(1-y)\sin\gamma, \tag{14}$$

$$T_{\mathrm{B}}(x,y,z) = Ra_{\mathrm{h}}\,(x\,\cos\gamma + z\,\sin\gamma) + Ra\,(1-y) - \frac{Ra_{\mathrm{h}}^2}{12}\left[Ge\,y^4 - 2\,(2\,Ge-1)y^3 + 6\,(Ge-1)y^2 - 3\,Ge + 4\right], \tag{15}$$

$$p_{\mathrm{B}}(x,y,z) = -\,Ra_{\mathrm{h}}\,(x\,\cos\gamma + z\,\sin\gamma)\,(1-y) - \frac{1}{2}\,Ra\,(1-y)^2 - \frac{Ra_{\mathrm{h}}^2}{120}\,(1-y)^2\left[2\,Ge\,y^3 - (6\,Ge-5)\,y^2 + 2\,(3\,Ge-5)\,y + 18\,Ge - 25\right], \tag{16}$$

where B stands for basic solution. In Fig. 2, plots of the reduced temperature difference,

$$\tilde{T}_{\mathrm{B}}(y) = \frac{T_{\mathrm{B}}(x,y,z) - T_{\mathrm{B}}(x,1,z)}{Ra_{\mathrm{h}}^2} = \frac{Ra}{Ra_{\mathrm{h}}^2}\,(1-y) - \frac{1}{12}\left[Ge\,y^4 - 2\,(2\,Ge-1)\,y^3 + 6\,(Ge-1)\,y^2 - 3\,Ge + 4\right], \tag{17}$$

are given for different values of Ge and of the ratio Ra/Ra_{h}^2. The four frames represented in Fig. 2 display the continuous transition from the regime $Ra/Ra_{\mathrm{h}}^2 \to 0$, where the system has a stable thermal stratification in the vertical direction, to the regime of large Ra/Ra_{h}^2, where the temperature distribution decreases linearly from the lower boundary $y = 0$ to the upper boundary $y = 1$. In the former regime ($Ra/Ra_{\mathrm{h}}^2 \to 0$), no thermal instability may occur, while in the latter regime ($Ra/Ra_{\mathrm{h}}^2 \gg 1$), the vertical thermal stratification is possibly unstable. We notice that the plots in the frame for $Ra/Ra_{\mathrm{h}}^2 = 100$ overlap thus revealing a poor influence of Ge and, hence, of the effect of viscous dissipation. The regime $Ra/Ra_{\mathrm{h}}^2 \to 0$ may correspond either to an adiabatic lower boundary or to an extremely large temperature gradient imposed horizontally through the upper boundary ($q_{\mathrm{h}} \to \infty$). We mention that, if $Ra/Ra_{\mathrm{h}}^2 \to 0$, the stable thermal stratification observed in Fig. 2 occurs only for $Ge \le 1$. In fact, from Eq. 17, one may easily prove that, for $1 < Ge < 3/2$, there exists a region adjacent to $y = 0$ where $\partial T_{\mathrm{B}}/\partial y < 0$ (possibly unstable stratification) and that, for $Ge \ge 3/2$, this region extends to the whole domain $0 < y < 1$. We note that the Gebhart number, Ge, is usually less than 1, and, in several practical cases, it is significantly less than 1. Then, the value $Ge = 3/2$ is definitely a huge one in most applications even if, in the existing literature, cases with even higher values of Ge have been considered (Turcotte et al. 1974). In the following, our investigation will be restricted to the range $Ge \le 1$: an extremely wide range for all practical purposes.

Whatever is the value of Ra/Ra_{h}^2, the basic temperature difference between the lower and the upper boundary tends to increase with Ge. As it can be easily shown from Eq. 15, the temperature difference between the lower and the upper boundary becomes positive when

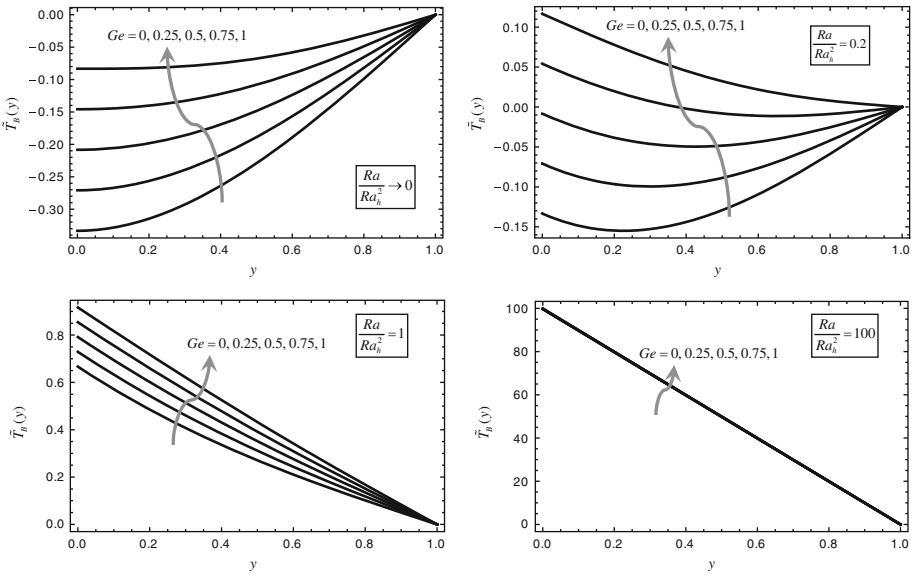

Fig. 2 Basic flow: reduced temperature distribution for different values of Ge and Ra_{h}^2/Ra

$$Ge > \frac{4}{3} - 4\,\frac{Ra}{Ra_{\mathrm{h}}^2}. \tag{18}$$

4 Linear Disturbances

A linear stability analysis of the basic solution is carried out to determine the conditions for the onset of convective rolls. In order to eliminate the pressure p from the governing equations, we evaluate the curl of Eq. 7, which yields

$$\frac{\partial w}{\partial y} - \frac{\partial v}{\partial z} = -\frac{\partial T}{\partial z}, \qquad \frac{\partial u}{\partial z} - \frac{\partial w}{\partial x} = 0, \qquad \frac{\partial v}{\partial x} - \frac{\partial u}{\partial y} = \frac{\partial T}{\partial x}. \tag{19}$$

We perturb the basic solution by setting

$$\mathbf{u} = \mathbf{u}_{\mathrm{B}} + \varepsilon \mathbf{U}, \qquad T = T_{\mathrm{B}} + \varepsilon\theta, \tag{20}$$

where ε is an arbitrarily small perturbation parameter, while $\mathbf{U}$ and θ are the velocity and temperature disturbances, respectively. Substitution of Eq. 20 into Eqs. 6, 8 and 19, by taking into account Eqs. 14 and 15, and neglecting terms of order ε^2, yields the following set of equations for the disturbances:

$$\frac{\partial U}{\partial x} + \frac{\partial V}{\partial y} + \frac{\partial W}{\partial z} = 0, \tag{21}$$

$$\frac{\partial W}{\partial y} - \frac{\partial V}{\partial z} = -\frac{\partial \theta}{\partial z}, \tag{22}$$

$$\frac{\partial U}{\partial z} - \frac{\partial W}{\partial x} = 0, \tag{23}$$

$$\frac{\partial V}{\partial x} - \frac{\partial U}{\partial y} = \frac{\partial \theta}{\partial x}, \tag{24}$$

$$\begin{aligned} &\frac{\partial \theta}{\partial t} + Ra_{\mathrm{h}}(1-y)\left(\cos\gamma\,\frac{\partial \theta}{\partial x} + \sin\gamma\,\frac{\partial \theta}{\partial z}\right) \\ &\quad + Ra_{\mathrm{h}}\,(U\cos\gamma + W\sin\gamma) + G(y)\,V = \frac{\partial^2\theta}{\partial x^2} + \frac{\partial^2\theta}{\partial y^2} + \frac{\partial^2\theta}{\partial z^2} \\ &\quad + 2\,Ge\,Ra_{\mathrm{h}}\,(1-y)\,(U\cos\gamma + W\sin\gamma), \end{aligned} \tag{25}$$

subject to the boundary conditions

$$\begin{aligned} y = 0: &\qquad V = 0, \quad \frac{\partial \theta}{\partial y} = 0, \\ y = 1: &\qquad U = W = 0, \quad \theta = 0, \end{aligned} \tag{26}$$

where

$$G(y) = \frac{\partial T_{\mathrm{B}}}{\partial y} = -Ra - \frac{Ra_{\mathrm{h}}^2}{12}\left[4\,Ge\,y^3 - 6\,(2\,Ge - 1)y^2 + 12\,(Ge - 1)y\right]. \tag{27}$$

5 Stability Equations with Respect to Rolls

Solutions of the disturbance Eqs. 21–26 are sought in the form of periodic rolls. Given that the angle γ is arbitrary, it is not restrictive to consider rolls with axes along the z-direction by first setting,

$$U = U(x, y, t), \qquad V = V(x, y, t), \qquad W = 0, \qquad \theta = \theta(x, y, t). \tag{28}$$

As a consequence, assuming $\gamma = 0$ implies the analysis of transverse rolls with axis orthogonal to the direction of the basic velocity. On the other hand, assuming $\gamma = \pi/2$ implies the study of longitudinal rolls with axis parallel to the direction of the basic velocity. Oblique rolls are such that $0 < \gamma < \pi/2$.

Equations 22 and 23 are satisfied identically and, by defining a stream function ψ,

$$U = \frac{\partial \psi}{\partial y}, \qquad V = -\frac{\partial \psi}{\partial x}, \tag{29}$$

also Eq. 21 is fulfilled. Moreover, Eqs. 24 and 25 can be rewritten in the form

$$\frac{\partial^2\psi}{\partial x^2} + \frac{\partial^2\psi}{\partial y^2} = -\frac{\partial \theta}{\partial x}, \tag{30}$$

$$\begin{aligned} &\frac{\partial \theta}{\partial t} + Ra_{\mathrm{h}}\,(1-y)\,\cos\gamma\,\frac{\partial \theta}{\partial x} + Ra_{\mathrm{h}}\cos\gamma\,\frac{\partial \psi}{\partial y} - G(y)\,\frac{\partial \psi}{\partial x} \\ &\quad = \frac{\partial^2\theta}{\partial x^2} + \frac{\partial^2\theta}{\partial y^2} + 2\,Ge\,Ra_{\mathrm{h}}\,(1-y)\,\cos\gamma\,\frac{\partial \psi}{\partial y}. \end{aligned} \tag{31}$$

The corresponding boundary equations are deduced from Eq. 26

$$\begin{aligned} y = 0: &\qquad \frac{\partial \psi}{\partial x} = 0, \quad \frac{\partial \theta}{\partial y} = 0, \\ y = 1: &\qquad \frac{\partial \psi}{\partial y} = 0, \quad \theta = 0. \end{aligned} \tag{32}$$

Solutions of Eqs. 30–32 are sought in the form of plane waves

$$\psi(x, y, t) = \Re\left\{i\, f(y)\, e^{i(ax-\lambda t)}\right\}, \qquad \theta(x, y, t) = \Re\left\{h(y)\, e^{i(ax-\lambda t)}\right\}, \tag{33}$$

where $\Re$ stands for the real part of a complex function, a is a real wave number, and $\lambda = \lambda_R + i\,\lambda_I$ is a complex exponential growth rate to be determined. We will be interested in the threshold value for neutral stability, so that, hereafter, we will set $\lambda_I = 0$. By substituting Eq. 33 into Eqs. 30 and 31, we obtain the following set of ordinary differential equations:

$$f'' - a^2 f + a\, h = 0, \tag{34}$$

$$h'' - \left(a^2 - i\,\lambda_R\right) h + i\, Ra_{\rm h}\, \cos\gamma\, \left\{[2\, Ge\,(1-y) - 1]\, f' - (1-y)\, a\, h\right\} - a\, G(y)\, f = 0, \tag{35}$$

subject, on account of Eq. 32, to the boundary conditions

$$\begin{aligned} y = 0: &\quad f = h' = 0, \\ y = 1: &\quad f' = h = 0. \end{aligned} \tag{36}$$

On account of Eq. 27, the homogeneous differential problem defined by Eqs. 34–36 can be solved as an eigenvalue problem. More precisely, for prescribed values of $(a, \gamma, Ra_{\rm h}, Ge)$, we determine (λ_R, Ra) as the eigenvalue pair corresponding to the eigenfunction pair (f, h). Thus, one may define a function $Ra(a)$ for any choice of $(\gamma, Ra_{\rm h}, Ge)$. Since we have chosen $\lambda_I = 0$, function $Ra(a)$ describes the neutral stability condition. By seeking the minimum of $Ra(a)$, one may obtain the critical values $(a_{\rm cr}, Ra_{\rm cr})$ for the onset of convective instability.

5.1 Numerical Solution

The eigenvalue problem defined by Eqs. 34–36 can be solved numerically by adopting the Runge–Kutta method. This numerical procedure is easily implemented in the Mathematica 7.0 (© Wolfram, Inc.) environment by using the built-in function `NDSolve`. The step size is controlled through an adaptive algorithm, and the differential order of the Runge–Kutta method by default is not specified by the user, but assigned by the system to optimise the numerical solution. The differential problem needs to be formulated as an initial value problem by completing the conditions at $y = 0$ defined by Eq. 36 as follows:

$$f(0) = 0, \qquad f'(0) = 1, \qquad h(0) = \eta, \qquad h'(0) = 0. \tag{37}$$

Since Eqs. 34–36 are homogeneous, the condition $f'(0) = 1$ is justified as a normalisation condition to break the scale invariance of the solution, (f, h). The complex parameter $\eta = \eta_R + i\,\eta_I$ is obviously an unknown and can be determined, through a shooting method, by means of the constraints

$$f'(1) = 0, \qquad h(1) = 0, \tag{38}$$

i.e. the boundary conditions, Eq. 36, at $y = 1$.

6 Discussion of the Results

6.1 The Limiting Case $Ra_h \to 0$

A special limiting case is $Ra_h \to 0$. In this limit, the basic solution Eqs. 14–17 is one of vanishing velocity and such that the temperature gradient is purely vertical and uniform. In particular, as it can be easily inferred from Eq. 10, this means that the upper boundary, $y = 1$, is isothermal in this case.

Equations 27, 34–36 reveal that the eigenvalue problem becomes independent of the inclination angle γ, in the limit $Ra_h \to 0$. This is an obvious consequence due to the absence of a basic horizontal flow, implying that all horizontal directions are equivalent. Finally, if $Ra_h \to 0$, the eigenvalue problem Eqs. 34–36 can be made self-adjoint by setting $\lambda_R = 0$. In other words, when $Ra_h \to 0$, we recover one of the many variants of the classical Darcy-Bénard problem discussed in Nield and Bejan (2006). In fact, on p. 194 of Nield-Bejan's book, one may find the critical values of a and Ra corresponding to a porous layer having: impermeable lower wall at uniform heat flux; and upper boundary surface at uniform pressure and temperature. The critical values reported in Nield and Bejan (2006), in this case, are

$$a_{cr} = 1.75, \qquad Ra_{cr} = 17.65. \tag{39}$$

This result was originally obtained in Nield (1968).

On solving numerically Eqs. 34–36 in the limit $Ra_h \to 0$, by means of the Runge–Kutta procedure described in Sect. 5.1, we get

$$a_{cr} = 1.749861, \qquad Ra_{cr} = 17.65365. \tag{40}$$

Finally, we note that, in the limit $Ra_h \to 0$, the eigenvalue problem Eqs. 34–36 is independent of Ge. This means that the viscous dissipation does not affect the solution of the disturbance equations when the basic state is such that the velocity field vanishes. More precisely, when $Ra_h \to 0$, the viscous dissipation becomes an higher-order effect, negligible when studying the linear stability.

6.2 Longitudinal Rolls

When considering longitudinal rolls, for which $\gamma = \pi/2$, the system of ordinary differential equations 34 and 35 is made self-adjoint by setting $\lambda_R = 0$. Equations 34 and 35 are now replaced by the following system:

$$f'' - a^2 f + a\, h = 0, \tag{41}$$

$$h'' - a^2 h - a\, G(y)\, f = 0. \tag{42}$$

Equations 41 and 42 subject to the boundary conditions Eq. 36 may be solved by a power series method using

$$f(y) = \sum_{n=0}^{\infty} \frac{A_n}{n!}\, y^n, \qquad h(y) = \sum_{n=0}^{\infty} \frac{B_n}{n!}\, y^n. \tag{43}$$

On applying the initial conditions specified in Eq. 37, we may write

$$A_0 = f(0) = 0, \qquad A_1 = f'(0) = 1, \qquad B_0 = h(0) = \eta, \qquad B_1 = h'(0) = 0, \tag{44}$$

Table 1 Comparison between the series solution and the Runge–Kutta method solution, for longitudinal rolls with $Ge = 0.5$

$Ra_{\rm h}$	$a_{\rm cr}$	$Ra_{\rm cr}$	$\eta_{\rm cr}$	Method
0	1.749853	17.65367	1.202617	Series, $N = 16$
0	1.749861	17.65365	1.202614	Series, $N = 18$
0	1.749861	17.65365	1.202614	Series, $N = 24$
0	1.749861	17.65365	1.202614	Series, $N = 30$
0	1.749861	17.65365	1.202614	Runge–Kutta
5	1.751322	23.06028	1.236445	Series, $N = 16$
5	1.751189	23.06065	1.236498	Series, $N = 18$
5	1.751179	23.06067	1.236501	Series, $N = 24$
5	1.751179	23.06067	1.236501	Series, $N = 30$
5	1.751179	23.06067	1.236501	Runge–Kutta
10	1.777987	39.04145	1.324611	Series, $N = 16$
10	1.775016	39.05113	1.325799	Series, $N = 18$
10	1.774851	39.05123	1.325855	Series, $N = 24$
10	1.774851	39.05123	1.325855	Series, $N = 30$
10	1.774851	39.05123	1.325855	Runge–Kutta
50	4.959338	354.9461	1.437904	Series, $N = 38$
50	4.956589	354.9683	1.438405	Series, $N = 44$
50	4.956714	354.9678	1.438385	Series, $N = 50$
50	4.956715	354.9678	1.438385	Series, $N = 56$
50	4.956715	354.9678	1.438385	Runge–Kutta

where η is a real parameter in this case, since the eigenvalue problem is self-adjoint. Higher order coefficients A_n and B_n may be determined by substituting expressions (43) into Eqs. 41 and 42 and collecting like powers of y. We thus obtain

$$B_2 = a^2\,\eta, \qquad B_3 = -a\,Ra, \qquad B_4 = a^4\,\eta + a^2\,Ra\,\eta - 2\,a\,Ra_{\rm h}^2\,(Ge - 1), \tag{45}$$

and the recursion relations

$$\begin{aligned} A_{n+2} &= a^2\,A_n - a\,B_n, \qquad n = 0, 1, 2, \ \ldots\ , \\ B_{n+2} &= a^2\,B_n - a\,Ra\,A_n - a\,Ra_{\rm h}^2\,[n\,(Ge - 1)\,A_{n-1} \\ &\quad -\tfrac{1}{2}\,n\,(n-1)\,(2\,Ge - 1)\,A_{n-2} + \tfrac{1}{3}\,n\,(n-1)\,(n-2)\,Ge\,A_{n-3}], \\ &\quad n = 3, 4, 5, \ \ldots\ . \end{aligned} \tag{46}$$

The above described power series solution may be used as a validation of the numerical solution procedure based on the Runge–Kutta method, discussed in Sect. 5.1. Table 1 displays a comparison between the series solution truncated to the first N terms and the Runge–Kutta solution. The comparison refers to the critical values of a, Ra and η, for $Ge = 0.5$ and $Ra_{\rm h} = 0, 5, 10, 50$. Different truncation numbers N are considered from 16 to 56. Table 1 clearly shows that, with $Ra_{\rm h} = 0, 5, 10$, the truncated series solution perfectly agrees with the Runge–Kutta solution within seven significant digits, if $N = 24$ and $N = 30$. More terms ($N = 56$) are needed for achieving convergence within seven significant digits in the case $Ra_{\rm h} = 50$. Then, we may conclude that the series solution displays a fast convergence and that the solution based on the Runge–Kutta method is definitely reliable. As a consequence of this validation procedure, all the subsequent numerical results will be based on the Runge–Kutta method.

6.3 Oblique Rolls with a Negligible Viscous Dissipation

The case of flow with a negligible viscous dissipation corresponds to the limit $Ge \to 0$. Figure 3 displays the change with γ of the ratio between the critical Rayleigh number, $Ra_{\rm cr}$,

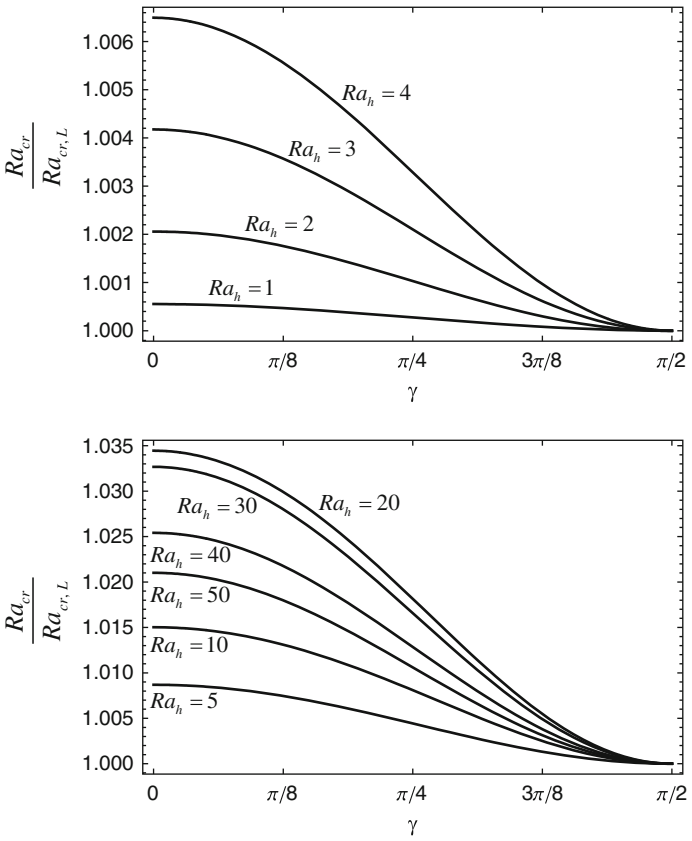

Fig. 3 Case $Ge = 0$: change of $Ra_{\mathrm{cr}}/Ra_{\mathrm{cr,L}}$ with γ for oblique rolls corresponding to different Ra_{h}

and the critical Rayleigh number for longitudinal rolls, $Ra_{\mathrm{cr,L}}$. This figure reveals that, for all the cases examined, the longitudinal rolls ($\gamma = \pi/2$) are more unstable than any other oblique rolls ($0 \leq \gamma < \pi/2$). When shifting from longitudinal to transverse rolls, the relative increment of Ra_{cr} increases with Ra_{h}, except for the cases with $Ra_{\mathrm{h}} > 10$. Among the cases examined in Fig. 3, this relative increment ranges from less than 0.1%, if $Ra_{\mathrm{h}} = 1$, to more than 3%, if $Ra_{\mathrm{h}} = 20$. The discussion carried out in Sect. 6.1 evidences that Ra_{cr} is the same for longitudinal, oblique and transverse rolls when $Ra_{\mathrm{h}} \to 0$.

Table 2, referring to longitudinal rolls, reveals the monotonic increasing trend of Ra_{cr} vs. Ra_{h}. This table contains the critical values of a, Ra and η for a horizontal Rayleigh number lying in the range $0 \leq Ra_{\mathrm{h}} \leq 50$. Table 2 shows also that the relative changes of a_{cr} and η_{cr} with Ra_{h} are definitely smaller than the relative change of Ra_{cr} with Ra_{h}.

We mention that a problem, similar to that examined in the present article, where both the boundaries are impermeable, the lower boundary is adiabatic and a uniform, horizontal temperature gradient is prescribed at the upper boundary has been recently studied in Barletta et al. (2010). The longitudinal rolls were found to be the most unstable with critical values of a and Ra_{h} given by

$$a_{\mathrm{cr}} = 2.622468, \qquad Ra_{\mathrm{h,cr}} = 15.03109. \tag{47}$$

Table 2 Case $Ge = 0$: critical values of a, Ra and η for longitudinal rolls with different Ra_h

Ra_h	a_{cr}	Ra_{cr}	η_{cr}
0	1.749861	17.65365	1.202614
0.5	1.749856	17.74133	1.203117
1	1.749845	18.00433	1.204624
2	1.749855	19.05565	1.210614
3	1.750070	20.80550	1.220468
4	1.750791	23.25032	1.233991
5	1.752442	26.38509	1.250915
6	1.755585	30.20330	1.270895
7	1.760932	34.69680	1.293515
8	1.769377	39.85566	1.318277
9	1.782041	45.66789	1.344597
10	1.800349	52.11900	1.371785
12	1.861791	66.86293	1.425307
15	2.062874	93.15686	1.485328
20	2.803035	144.6343	1.477090
25	3.498291	200.5975	1.455364
30	4.037864	260.2296	1.452434
35	4.536974	323.5775	1.450809
40	5.017779	390.3085	1.448600
45	5.478522	460.0966	1.446714
50	5.920623	532.6999	1.445269

The problem studied in the present article admits a limiting case where the lower boundary is adiabatic, i.e., the case $Ra \to 0$. In this limit, the thermal boundary conditions are exactly the same as in Barletta et al. (2010), the only difference being the upper impermeable boundary (Barletta et al. 2010) instead of the upper open boundary (present article). However, this difference has dramatic consequences. In fact, if $Ra \to 0$, with an upper open boundary, we cannot have any thermal instability as the basic temperature profile evidences a stable thermal stratification in the vertical y-direction. A representation of this behaviour is given in Fig. 2 in the frame referring to the case $Ra/Ra_h^2 \to 0$. A comparison between the results reported in Barletta et al. (2010) and those discussed in this section allows one to conclude that a non-vanishing horizontal temperature gradient has a destabilising effect in the case of an upper impermeable boundary (Barletta et al. 2010), while it has a stabilising effect if the plane $y = 1$ is an open boundary. In fact, in the case of an upper impermeable boundary (Barletta et al. 2010), the basic velocity has the direction opposite to that of the imposed horizontal temperature gradient. On the contrary, Eqs. 14 and 15 reveal that, with an upper open boundary, the basic velocity has the same direction as the imposed horizontal temperature gradient. This means that, with an upper impermeable boundary, the basic solution is such that the fluid experiences a streamwise cooling from the upper boundary. On the other hand, with an upper open boundary, the basic solution is such that the fluid is heated from the upper boundary in the streamwise direction. This simple fact justifies, on physical grounds, the different effects of the horizontal temperature gradient: destabilising for the upper impermeable boundary; stabilising for the upper open boundary.

Figure 4 displays the streamlines $\psi = constant$ and the isotherms $\theta = constant$ for longitudinal rolls under critical conditions with $Ra_h = 0, 10, 20, 50$. The complete critical data in these two cases can be easily obtained from Table 2. Figure 4 reveals that, on increasing Ra_h, the convective rolls become more and more compressed to the lower boundary $y = 0$. Moreover, this figure displays the effect of the homogeneous

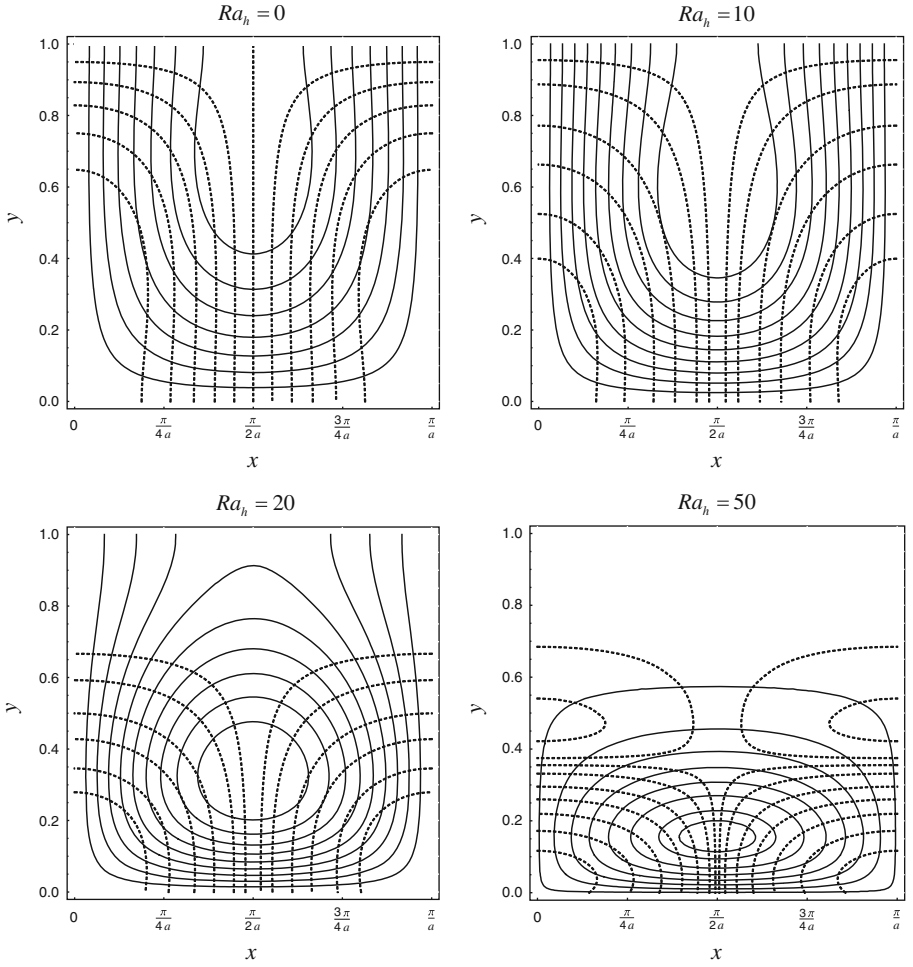

Fig. 4 Case $Ge = 0$: streamlines $\psi = constant$ (*solid lines*) and isotherms $\theta = constant$ (*dashed lines*) for longitudinal rolls under critical conditions with $Ra_{\mathrm{h}} = 0, 10, 20, 50$

boundary conditions on the disturbances: Dirichlet and Neumann conditions on ψ and θ, respectively, at $y = 0$; and Neumann and Dirichlet conditions on ψ and θ, respectively, at $y = 1$.

6.4 Oblique Rolls with a Non-Negligible Viscous Dissipation

When the Gebhart number is nonzero, the effect of the viscous dissipation is taken into account. In order to span a wide range of $Ge \neq 0$, Fig. 5 refers to the four values $Ge = 0.25, 0.5, 0.75, 1$, while the curves for $Ge = 0$ serve for comparison. Figure 5 suggests that, even with an important effect of viscous dissipation, the longitudinal roll disturbances are the most unstable. This conclusion is taken from the plots in the frames referring to $Ra_{\mathrm{h}} = 10, 20, 50$. From Fig. 5, one may deduce that, generally, the discrepancy between the

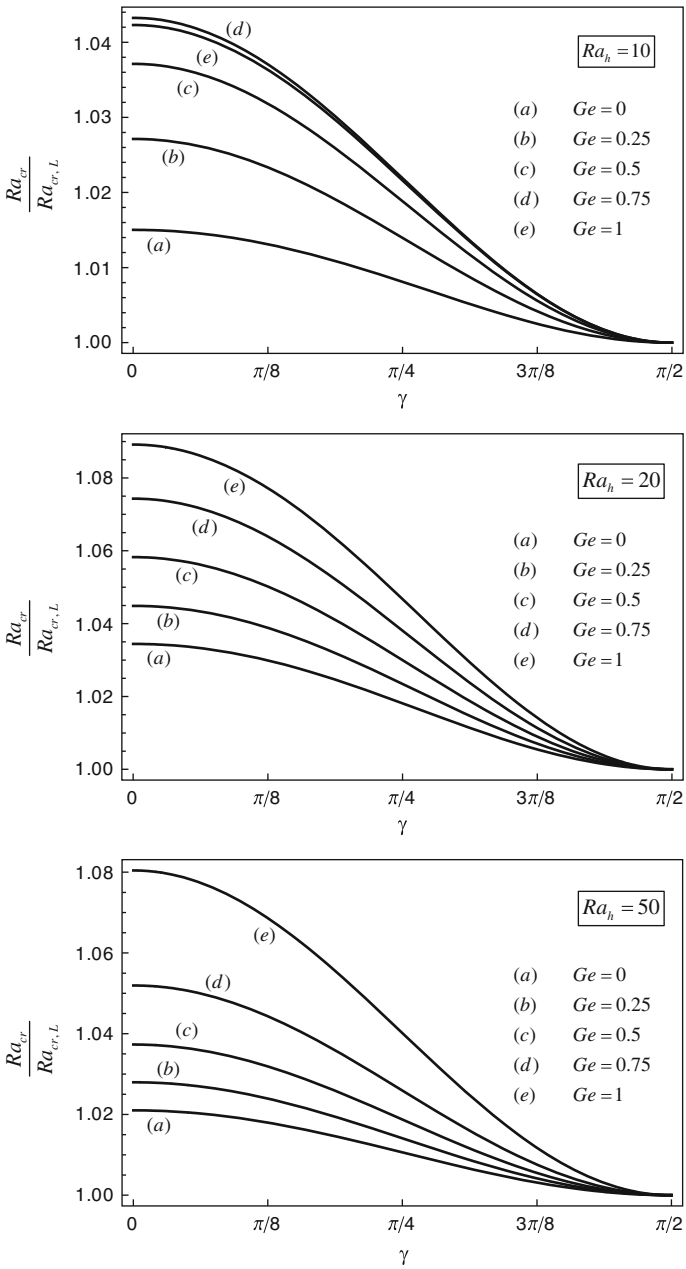

Fig. 5 Change of $Ra_{\rm cr}/Ra_{\rm cr,L}$ with γ for oblique rolls corresponding to $Ra_{\rm h} = 10, 20, 50$

critical Rayleigh number for longitudinal rolls increases with Ge. There is just an exception to this rule, when $Ra_{\rm h} = 10$ and $Ge = 0.75, 1$.

The critical values $a_{\rm cr}$ and $Ra_{\rm cr}$ for longitudinal rolls and different values of Ge and $Ra_{\rm h}$ are reported in Table 3. This table shows the monotonic dependence of the critical parameter

Table 3 Critical values of a and Ra for longitudinal rolls with different Ra_h and Ge

Ra_h	$Ge = 0.25$	$Ge = 0.5$	$Ge = 0.75$	$Ge = 1$	
0	1.749861	1.749861	1.749861	1.749861	a_{cr}
	17.65365	17.65365	17.65365	17.65365	Ra_{cr}
1	1.749849	1.749853	1.749857	1.749862	a_{cr}
	17.93749	17.87066	17.80382	17.73697	Ra_{cr}
2	1.749855	1.749859	1.749866	1.749876	a_{cr}
	18.78850	18.52131	18.25408	17.98681	Ra_{cr}
5	1.751745	1.751179	1.750743	1.750436	a_{cr}
	24.72365	23.06067	21.39616	19.73014	Ra_{cr}
7	1.757934	1.755466	1.753515	1.752072	a_{cr}
	31.45926	28.21569	24.96614	21.71068	Ra_{cr}
10	1.786300	1.774851	1.765836	1.759118	a_{cr}
	45.59888	39.05123	32.47705	25.87714	Ra_{cr}
12	1.829523	1.803786	1.783869	1.769198	a_{cr}
	57.59532	48.26374	38.87251	29.42504	Ra_{cr}
15	1.966324	1.892139	1.837098	1.798025	a_{cr}
	79.11212	64.85967	50.42829	35.83976	Ra_{cr}
20	2.540372	2.279459	2.062989	1.912674	a_{cr}
	122.1328	98.64841	74.25982	49.13614	Ra_{cr}
25	3.233194	2.919694	2.551159	2.183717	a_{cr}
	169.4877	136.6940	101.8775	64.86089	Ra_{cr}
30	3.754312	3.439963	3.069613	2.611269	a_{cr}
	219.5248	176.5736	130.8236	81.51785	Ra_{cr}
35	4.207470	3.854119	3.467528	3.010908	a_{cr}
	272.4431	218.3043	160.4797	97.93886	Ra_{cr}
40	4.641859	4.233549	3.796220	3.320399	a_{cr}
	328.1296	262.0245	191.0711	113.9866	Ra_{cr}
45	5.061496	4.600773	4.099144	3.571158	a_{cr}
	386.3296	307.6320	222.7165	129.8661	Ra_{cr}
50	5.464964	4.956715	4.392086	3.792730	a_{cr}
	446.8318	354.9678	255.3884	145.7290	Ra_{cr}

Ra_{cr} on both Ge and Ra_h. Both Tables 2 and 3 reveal that, for small values of Ra_h, a_{cr} is a weakly non-monotonic function of Ra_h and a weakly increasing function of Ge. This behaviour is quite different from that inferred from these tables for $Ra_h > 2$, namely a_{cr} is an increasing function of Ra_h and a decreasing function of Ge.

Figures 6–8 refer to longitudinal rolls and display the behaviour of Ra_{cr} and a_{cr}. On considering fixed values of Ge, Fig. 6 displays the monotonic increasing trends of both Ra_{cr} and a_{cr} as functions of Ra_h. This figure evidences the destabilising effect of the viscous dissipation, as the increase of Ra_{cr} with Ra_h is steeper for smaller values of Ge. For assigned values of Ra_h, the changes of Ra_{cr} and of a_{cr} with Ge are illustrated in Figs. 7 and 8. These figures show clearly that both Ra_{cr} and a_{cr} are decreasing functions of Ge. This means that the flow becomes more and more unstable if the Gebhart number increases, i.e., if the viscous dissipation effect becomes more and more intense, as it can be inferred from Eq. 8. As a general criterion, Figs. 7 and 8 reveal that the parameter Ge has an increasing influence on the critical data (a_{cr}, Ra_{cr}) when the value of Ra_h increases. This is, in fact, a reasonable feature if one remembers that, on account of Eq. 14, the intensity of the basic horizontal flow is governed by the parameter Ra_h. As a consequence, the intensity of the viscous heating contribution grows with Ra_h^2, as it can be deduced from Eq. 15.

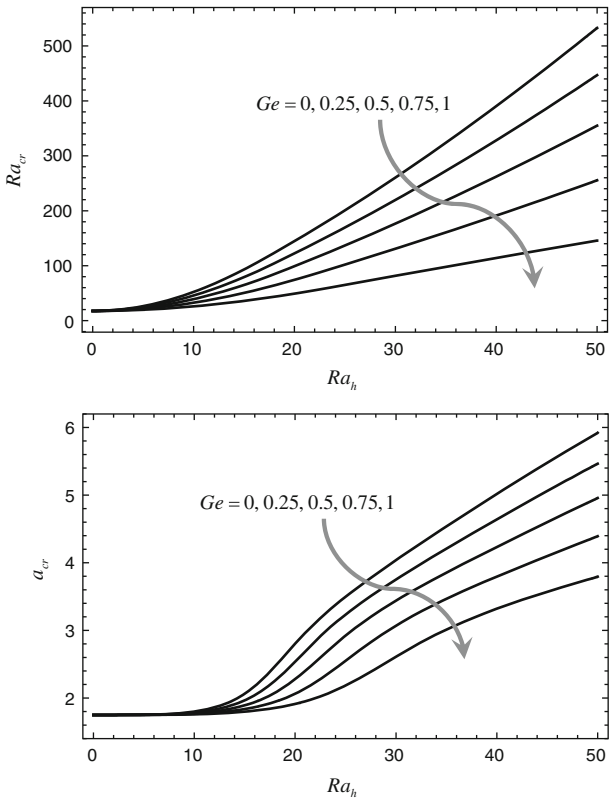

Fig. 6 Plots of $Ra_{\rm cr}$ (*upper frame*) and $a_{\rm cr}$ (*lower frame*) vs. $Ra_{\rm h}$ for longitudinal rolls corresponding to different values of Ge

7 Conclusions

A basic parallel Darcy flow in a horizontal porous layer, such that the seepage velocity profile is non-uniform, has been considered. The lower boundary is impermeable while the upper boundary is an open, constant pressure, surface. The basic flow is buoyancy induced, due to an imposed oblique temperature gradient. The basic temperature gradient is caused by the uniform heating on the lower boundary wall, governed by the Rayleigh number Ra, by the linearly changing temperature on the upper open boundary, governed by the horizontal Rayleigh number $Ra_{\rm h}$, and by the effect of the viscous dissipation, governed by the Gebhart number Ge. A linear stability analysis of the basic flow has been carried out, by considering oblique roll disturbances arbitrarily oriented with respect to the basic seepage velocity distribution. Limiting cases are the longitudinal rolls with axis parallel to the basic velocity, and transverse rolls with axis orthogonal to the basic velocity. The governing equations for the linear disturbances have been solved numerically by a Runge–Kutta method. The method has been validated using a power series solution of the disturbance equations in the case of longitudinal rolls.

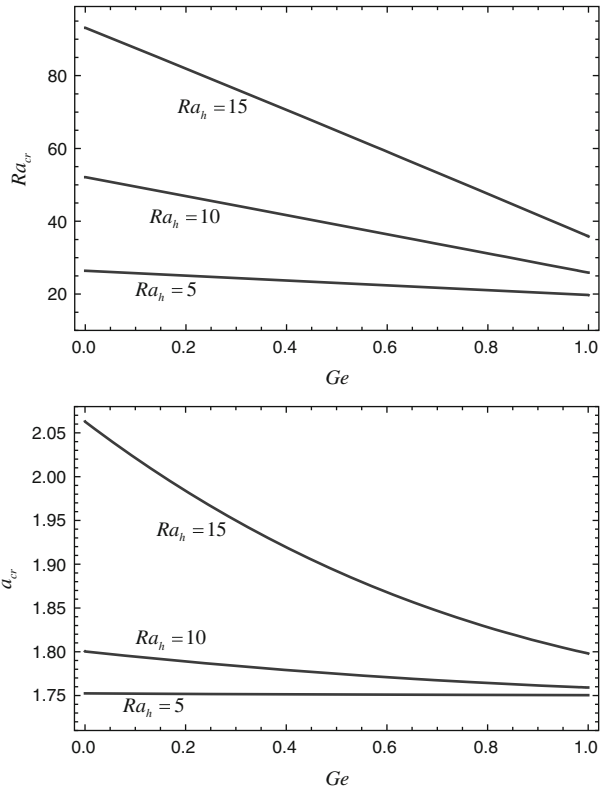

Fig. 7 Plots of Ra_{cr} (*upper frame*) and a_{cr} (*lower frame*) vs. Ge for longitudinal rolls corresponding to $Ra_{\mathrm{h}} = 5, 10, 15$

Among the results obtained, we mention the following:

(a) In all the cases examined, the basic buoyant flow is more unstable to longitudinal rolls than to any other oblique roll disturbance. The eigenvalue problem for longitudinal rolls is self-adjoint.

(b) In the special case $Ra_{\mathrm{h}} \to 0$, the basic solution and the linear stability analysis are not affected by the viscous dissipation, i.e. they are independent of the Gebhart number. The motionless basic solution becomes unstable when the Rayleigh number exceeds the critical value $Ra_{\mathrm{cr}} = 17.65365$. In this limit, the stability analysis coincides with that carried out in Nield (1968).

(c) If the viscous dissipation can be neglected, $Ge \to 0$, the basic flow becomes unstable when the Rayleigh number exceeds a critical value, Ra_{cr}, that depends on the prescribed horizontal Rayleigh number, Ra_{h}. The value Ra_{cr} is a monotonic increasing function of Ra_{h}.

(d) The effect of the viscous dissipation is destabilising. This means that, for a given Ra_{h}, the value Ra_{cr} is a monotonic decreasing function of Ge. On the contrary, the imposed horizontal temperature gradient has a stabilising effect.

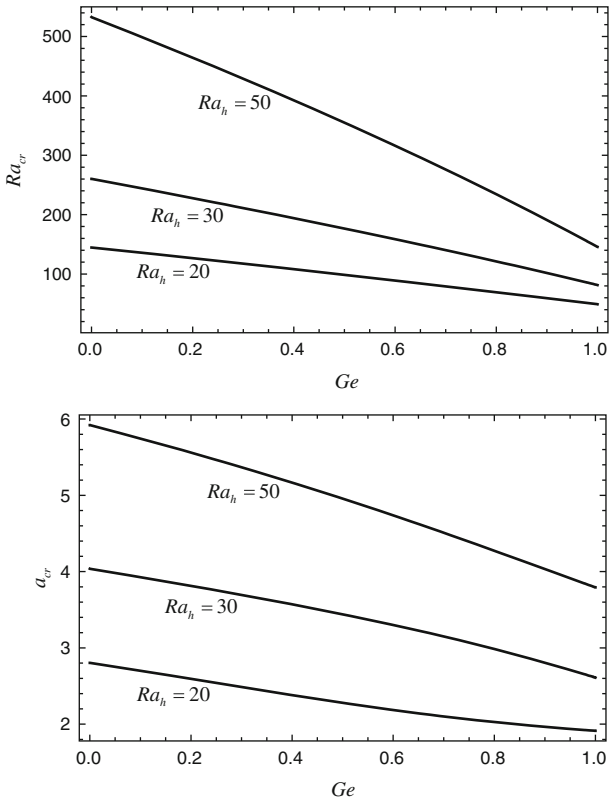

Fig. 8 Plots of $Ra_{\rm cr}$ (*upper frame*) and $a_{\rm cr}$ (*lower frame*) vs. Ge for longitudinal rolls corresponding to $Ra_{\rm h} = 20, 30, 50$

(e) In the limit $Ra \to 0$, corresponding to a thermally insulated lower wall, no instability may occur, if $Ge \leq 1$. Higher values of Ge may in fact correspond to a thermally unstable basic solution. However, such extremely high values of Ge are of minor practical interest and have not been considered in the present analysis.

References

Barletta, A.: Local energy balance, specific heats and the Oberbeck-Boussinesq approximation. Int. J. Heat Mass Transf. **52**, 5266–5270 (2009)

Barletta, A., Celli, M., Nield, D.A.: Unstably stratified Darcy flow with impressed horizontal temperature gradient, viscous dissipation and asymmetric thermal boundary conditions. Int. J. Heat Mass Transf. **53**, 1621–1627 (2010)

Elder, J.W.: Steady free convection in a porous medium heated from below. J. Fluid Mech. **27**, 29–48 (1967)

Horton, C.W., Rogers, F.T.: Convection currents in a porous medium. J. Appl. Phys. **16**, 367–370 (1945)

Lapwood, E.R.: Convection of a fluid in a porous medium. Proc. Camb. Philol. Soc. **44**, 508–521 (1948)

Laure, P., Roux, B.: Linear and non-linear analysis of the Hadley circulation. J. Cryst. Growth **97**, 226–234 (1989)

Lu, N., Zhang, Y., Ross, B.: Onset of gas convection in a moist porous layer with the top boundary open to the atmosphere. Int. Commun. Heat Mass Transf. **26**, 33–44 (1999)

McKibbin, R.: Thermal convection in a porous layer: effects of anisotropy and surface boundary conditions. Transp. Porous Media **1**, 271–292 (1986)
Nield, D.A.: Onset of thermohaline convection in a porous medium. Water Resour. Res. **4**, 553–560 (1968)
Nield, D.A., Bejan, A.: Convection in Porous Media 3rd edition. Springer-Verlag, New York (2006)
Prats, M.: The effect of horizontal fluid flow on thermally induced convection currents in porous mediums. J. Geophys. Res. **71**, 4835–4838 (1966)
Rees, D.A.S.: The effect of inertia on the onset of mixed convection in a porous layer heated from below. Int. Commun. Heat Mass Transf. **24**, 277–283 (1997)
Rees, D.A.S: The stability of Darcy-Bénard convection. In: Vafai, K. (ed.) Handbook of Porous Media, chapter 12, pp. 521–558. Marcel Dekker, New York (2000)
Rees, D.A.S.: The onset of Darcy-Brinkman convection in a porous layer: An asymptotic analysis. Int. J. Heat Mass Transf. **45**, 2213–2220 (2002)
Turcotte, D.L., Hsui, A.T., Torrance, K.E., Schubert, G.: Influence of viscous dissipation on Bénard convection. J. Fluid Mech. **64**, 369–374 (1974)
Tyvand, P.A: Onset of Rayleigh-Bénard convection in porous bodies. In: Ingham, D.B., Pop, I. (eds.) Transport Phenomena in Porous Media II, chapter 4, pp. 82–112. Pergamon, New York (2002)
Weber, J.E.: Convection in a porous medium with horizontal and vertical temperature gradients. Int. J. Heat Mass Transf. **17**, 241–248 (1974)